Journal of Power Sources 189 (2009) 89–94

Contents lists available at ScienceDirect

Journal of Power Sources

journal homepage: www.elsevier.com/locate/jpowsour

Fourier-transform infrared spectroscopic studies on the solid electrolyte interphase formed on Li-doped spinel $Li_{1.05}Mn_{1.96}O_4$ cathode

Chuan Wu[a,b,*], Ying Bai[a,b], Feng Wu[a,b]

[a] School of Chemical Engineering and the Environment, Beijing Institute of Technology, Beijing 100081, China
[b] National Development Center for High Technology Green Materials, Beijing 100081, China

ARTICLE INFO

Article history:
Received 14 August 2008
Received in revised form 18 October 2008
Accepted 4 November 2008
Available online 13 November 2008

Keywords:
Lithium ion batteries
Cathode
$Li_{1.05}Mn_{1.96}O_4$
Solid electrolyte interphase
Fourier-transform infrared spectroscopy

ABSTRACT

Fourier-transform infrared (FTIR) spectroscopy has been used to identify the solid electrolyte interphase (SEI) formed on Li-doped spinel $Li_{1.05}Mn_{1.96}O_4$ cathode. The major components in the SEI have been assigned, and the formation and evolution of the SEI over the initial charge–discharge cycle are discussed. By Fourier-transform infrared spectroscopy, it has been found that during the charge–discharge process, the SEI can be directly formed on the $Li_{1.05}Mn_{1.96}O_4$ cathode, and is mainly composed of R-CO_3Li and Li_2CO_3. In terms of composition, it is very similar to those formed on a carbon anode. In the initial cycle, the formation of R-CO_3Li begins at 4.10 V during the charging process, and becomes more distinct with increasing charge voltage. The formation of Li_2CO_3 begins at 4.10 V during the discharge process, and becomes more distinct with decreasing discharge voltage. The SEI becomes more evident over subsequent cycles.

1. Introduction

In 1970, Dey and Sullivan [1] found the intercalation of Li^+ into graphite to be accompanied by decomposition of the propylene carbonate (PC) used as solvent. It was reported by Fong et al. [2] that the amount of electrolyte decomposition is proportional to the specific surface area of the carbon electrode. Peled and Straze [3] and Peled [4] suggested that in practical nonaqueous battery systems, the alkali and alkaline earth metals are always covered with a surface layer, which is formed instantly by the reaction of the metal with the electrolyte and is named the solid electrolyte interphase (SEI). This is helpful in interpreting the irreversible capacity loss of the anodes during the initial cycle [5]. Though the compositions of the SEI formed on the anodes may change when different electrolytes are adopted [6–8], similar surface phenomena are observed on anode materials such as carbonaceous materials [9–23], metallic lithium [24,25], SnO [26], $Li_4Ti_5O_{12}$ [18], etc.

Chemical transformations of the electrode surfaces in lithium ion batteries between different cathodes and anodes have also been studied in recent years, and among such batteries those with $LiCoO_2$ cathodes and carbon anodes [27–29] have been the most extensively investigated. It was found that the SEI on the $LiCoO_2$ cathode was the same species [29] as that on a carbon anode. For a lithium ion battery assembled with an $LiMn_{1.7}Al_{0.3}O_4$ cathode and a hard carbon anode [30], the SEI was formed by decomposition products derived from $LiPF_6$, polymerized EC, and manganese dissociated from the $LiMn_{1.7}Al_{0.3}O_4$ cathode. For a lithium ion battery assembled with an $LiNi_{0.5}Mn_{1.5}O_4$ cathode and a graphite anode [31], it was demonstrated that proper SEI formation on the graphite anode substantially improved the electrochemical performance.

Generally, it is believed that the SEI may first be formed on the anode, then migrates with the electrolyte, and ultimately adheres to the cathode [8,32]. However, our interest has been in ascertaining whether the SEI can be formed directly on the cathode, i.e., if there is direct reaction at the cathode–electrolyte interface, and if this is similar to that at the anode–electrolyte interface. Recently, Edstrom et al. [33] used X-ray photoelectron spectroscopy (XPS) to probe the cathode-related SEI phenomena for $LiMn_2O_4$, $LiCoO_2$/$LiNi_{0.8}Co_{0.2}O_2$, and carbon-coated $LiFePO_4$. The results were related to the more familiar SEI layer formed on graphite. In the present study, Fourier-transform infrared spectroscopy has been used to identify the SEI formed on an Li-doped spinel $Li_{1.05}Mn_{1.96}O_4$ cathode. The major components in the SEI are assigned, and the formation and evolution of the SEI during the initial charge–discharge cycle are discussed.

2. Experimental

The Li-doped spinel $LiMn_2O_4$ was synthesized by a solid-state reaction as reported previously [34,35]. Lithium hydroxide

* Corresponding author at: School of Chemical Engineering and the Environment, Beijing Institute of Technology, Beijing 100081, China. Tel.: +86 10 68912657; fax: +86 10 68451429.
E-mail address: chuanwu@bit.edu.cn (C. Wu).

0378-7753/$ – see front matter © 2008 Elsevier B.V. All rights reserved.
doi:10.1016/j.jpowsour.2008.11.016

($LiOH{\cdot}H_2O$, 97%, Beijing Reagents) and chemical manganese dioxide (CMD, 85%, MMM, Belgium) were used as the raw materials. The nominal Li/Mn ratio was selected as 0.55:1. The raw materials were mixed and ground thoroughly, preheated at 480 °C for 8 h, reground and pressed into pellets, and then sintered at 750 °C for 24 h before being cooled in air.

The actual stoichiometry of the as-prepared sample was analyzed with an ICP spectrometer (IRIS/AP, Thermao Jarrell Ash). The oxygen content was estimated from the lithium and manganese contents. By this means, the stoichiometry of the sample was determined as Li:Mn:O = 1.05:1.96:4. The crystal structure of $Li_{1.05}Mn_{1.96}O_4$ was determined on a Rigaku Brmax-2400 X-ray diffractometer employing Cu Kα radiation. The scan range was from 10° to 100°, and the scan rate was selected as 8° min^{-1} in steps of 0.02°.

For charge–discharge tests, cathodes were prepared by coating slurries of spinel $Li_{1.05}Mn_{1.96}O_4$ powder, carbon black, and cyclopentanone-dissolved poly(vinylidene fluoride) (PVDF) onto aluminum foils, resulting in a weight ratio of $Li_{1.05}Mn_{1.96}O_4$, carbon black, and PVDF of 85:10:5. Subsequently, the films were vacuum-dried at 55 °C for 24 h, compressed between two stainless steel plates, and then cut into small sheets of area 0.5 cm^2. The as-prepared cathodes were assembled into Swagelok-type secondary lithium batteries in an argon-filled glove box (MBRAUN), using lithium metal foils as the counter and reference electrodes, and 1 mol L^{-1} $LiPF_6$ in a 1:1 (v/v) mixture of ethylene carbonate (EC) and diethyl carbonate (DEC) as the electrolyte (water content ≤20 ppm). Celgard® 2300 sheets were used as separators. The charge–discharge tests were performed on a LAND CT2001A battery tester. Before the charge–discharge tests, the batteries were aged for 12 h to ensure good soakage of the $Li_{1.05}Mn_{1.96}O_4$ particles in the cathode by the electrolyte. To ensure the SEI is formed just at the preconcerted voltage, for instance 4.21 V, the battery was charged at a constant current density of 0.4 mA cm^{-2} to 4.21 V, and then followed by a constant voltage of 4.21 V until the current decreased to 0.01 mA.

The collected Fourier-transform infrared (FTIR) spectra were the average of 100 scans obtained on an FTS-60V spectrometer (Bio-Rad) with a resolution of 4 cm^{-1}. Before recording the FTIR spectra of $Li_{1.05}Mn_{1.96}O_4$, the cathodes were carefully washed with DEC in the argon-filled glove box, and then transferred to a vacuum chamber to remove the solvent. Thereafter, the powders on the cathodes were collected, ground together with KBr, and then pressed into translucent pellets.

3. Results and discussion

3.1. Crystal structure of $Li_{1.05}Mn_{1.96}O_4$

Fig. 1 shows the XRD pattern of $Li_{1.05}Mn_{1.96}O_4$, which is accordance with reference [36] and indicates that the sample has a pure spinel $LiMn_2O_4$ phase with the *Fd3m* space group. Using the silicon peak at around 28° as a reference, the lattice parameter of $Li_{1.05}Mn_{1.96}O_4$ was calculated from the XRD pattern and was found to be 8.213 Å, which is very close to the 8.247 Å reported in Ref. [36].

3.2. Assignment of the SEI on $Li_{1.05}Mn_{1.96}O_4$

Fig. 2 shows the FTIR spectra of $Li_{1.05}Mn_{1.96}O_4$ cycled in 1 mol L^{-1} $LiPF_6$-EC/DEC. In the spectrum of the electrolyte, three peaks, at 1018 cm^{-1}, 846 cm^{-1}, and 559 cm^{-1}, are the characteristic absorptions of $LiPF_6$, while the other peaks may be assigned to the absorption bands of the EC/DEC solvent mixture. In spectra B, C, and D, the absorption bands from 625 cm^{-1} to 631 cm^{-1} are the characteristic vibrations of the Mn–O bonds in spinel $LiMn_2O_4$ [37]. The peak located at 846 cm^{-1} displays a red-shift with increasing cycle number, as shown in Fig. 2(a), indicating partial decomposition of $LiPF_6$ upon cycling, as described by Eqs. (1)–(3):

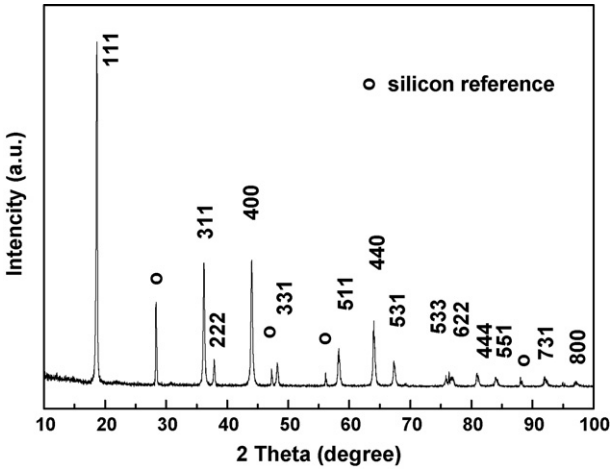

Fig. 1. XRD pattern of $Li_{1.05}Mn_{1.96}O_4$ synthesized via a solid-state reaction.

$$LiPF_6 \Leftrightarrow LiF \downarrow + PF_5 \quad (1)$$

$$PF_5 + H_2O \rightarrow 2HF + PF_3O \quad (2)$$

$$PF_3O + Li^+ + e^- \rightarrow LiF \downarrow + Li_xPOF_y \downarrow \quad (3)$$

However, because the vibrations of the residual electrolyte on $Li_{1.05}Mn_{1.96}O_4$ are very strong, the vibration of LiF at 775 cm^{-1} is overlapped by the CO_2 asymmetric bending of the EC/DEC solvent mixture.

The assignments of all of the absorption bands of $Li_{1.05}Mn_{1.96}O_4$ in different cycles are listed in Table 1. The weak peak located at 901 cm^{-1} is assigned to the CH_2 bending of the electrolyte. After the initial cycle, it becomes the shoulder peak at 841 cm^{-1}. With increasing cycle number, the electrolyte is gradually decomposed, and the absorption bands located between 897 and 901 cm^{-1} may be assigned to a combination of CO_3 bending in R-CO_3Li (R = methyl, ethyl) and Li_2CO_3.

Li_2CO_3 displays three strong vibration bands at 1510–1505 cm^{-1}, 1453 cm^{-1}, and 868 cm^{-1} [2]. For the $Li_{1.05}Mn_{1.96}O_4$ cathode after 1 cycle, only a weak peak at 1502 cm^{-1} is detected, while for the $Li_{1.05}Mn_{1.96}O_4$ cathodes after 5 and 10 cycles, distinct absorption bands at 1502 cm^{-1} and 1452 cm^{-1} appear, as shown in Fig. 2(d). This implies that Li_2CO_3, as one of the components in the solid electrolyte interphase, is already formed in the initial cycle, and increases with further cycling. The small amount of Li_2CO_3 may originate from the decomposition of DEC [8], as described by Eq. (4):

$$CH_3CH_2CO_3CH_2CH_3 + 2Li^+ + 2e^- \rightarrow Li_2CO_3 \downarrow + CH_3CH_2CH_2CH_3 \quad (4)$$

For the $LiPF_6$-EC/DEC electrolyte, the decomposition of solvent is a free radical terminating reaction [8], and may follow Eq. (5) to form R-CO_3Li on an Li metal anode. However, in this study, the appearance on the cathodes of R-CO_3Li originates from different routes, as described by Eqs. (6) and (7). It is clear that all of the cycled $Li_{1.05}Mn_{1.96}O_4$ cathodes display a new vibration peak at 1469 cm^{-1} in their spectra, which may be assigned to the CH(CH_3) asymmetric bending of R-CO_3Li (R = methyl, ethyl), as shown in Fig. 2(d). In Fig. 2(f), a new absorption band at 2846–2850 cm^{-1} (due to the CH stretch of R-CO_3Li) is more compelling evidence for the formation of R-CO_3Li (R = methyl, ethyl). In addition, for the $Li_{1.05}Mn_{1.96}O_4$ cath-

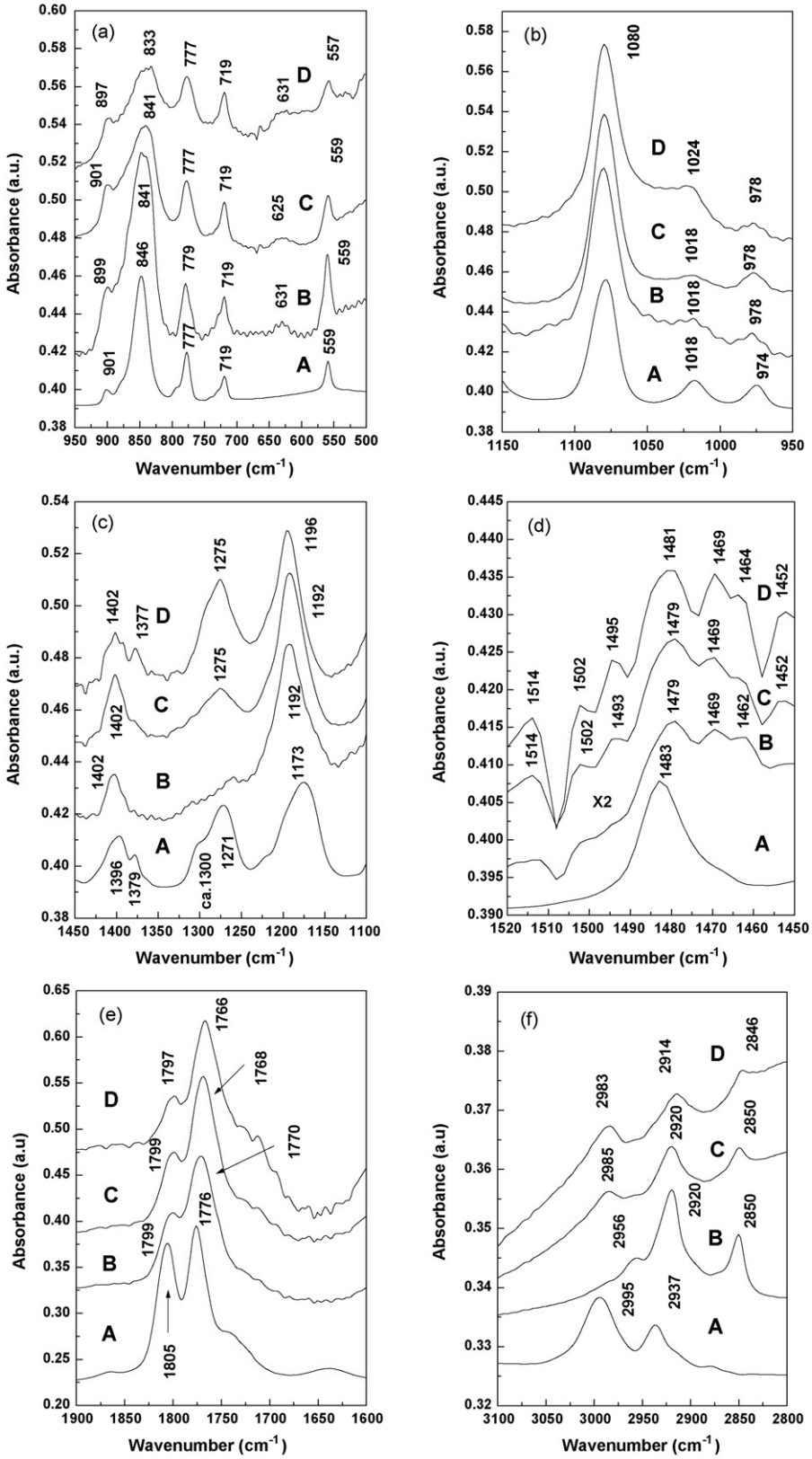

Fig. 2. FTIR spectra of $Li_{1.05}Mn_{1.96}O_4$ cathodes cycled in 1 mol L^{-1} $LiPF_6$-EC/DEC with a current density of 0.4 mA cm^{-2} in the voltage range 3–4.5 V. The figures exhibit the adsorption bands of the cycled $Li_{1.05}Mn_{1.96}O_4$ cathodes for various regions: (a) 950–500 cm^{-1}; (b) 1150–950 cm^{-1}; (c) 1450–1150 cm^{-1}; (d) 1500–1450 cm^{-1}; (e) 1900–1600 cm^{-1}; (f) 3100–2800 cm^{-1}. Curves A, B, C, D show 1 mol L^{-1} $LiPF_6$-EC/DEC and $Li_{1.05}Mn_{1.96}O_4$ cathodes after 1, 5 and 10 cycles, respectively.

Table 1
FTIR vibration modes and correspondent peak positions of $Li_{1.05}Mn_{1.96}O_4$ cycled in 1 mol L^{-1} $LiPF_6$-EC/DEC.

Vibration modes	Peak positions (cm^{-1})				
	EC/DEC	$LiPF_6$	$LiMn_2O_4$	Li_2CO_3	R-CO_3Li
CH stretch	2937w, 2995w				2846–2983w
CO_2 stretch	1805s, 1776s				
				1502w, 1402w	
CH, CH_3 asym. bend	1483m				1495w, 1493w, 1469–1462w, 1402m
CO_2 sym. bend	1396m, 1379sh				
CH_3 sym. bend	1271s				
CO stretch	1174s, 1080s				1192–1196s, 1080–1024s
		1018s			
CH_2 bend	974m, 901m				
		846s			
CO_3 bend				901–833s	901–833s
CO_2 asym. bend	777m, 719m				
MnO_6 asym. bend			631–625w		
		559m			

Note: w: weak; m: middle; s: strong; sh: shoulder.

ode after 10 cycles, a projection at the shoulder of the 1080 cm^{-1} peak is seen, indicating the emergence of new absorption bands in the range 1024–1080 cm^{-1}. These correspond to the CO stretching of R-CO_3Li, as shown in Fig. 2(b):

$$DEC + e^- + Li^0 \rightarrow CH_3CH_2^{\bullet} + CH_3CH_2OCO_2Li \downarrow \quad (5)$$

$$DEC + 2e^- + 2Li^+ \rightarrow LiCH_2CH_2CO_3CH_2CH_2Li \downarrow \quad (6)$$

$$EC + 2e^- + 2Li^+ \rightarrow LiCH_2CH_2OCO_2Li \downarrow \quad (7)$$

3.3. Formation and evolution of the SEI in the initial charge process

In order to further understand the formation and evolution of the SEI during the charge–discharge process, six $Li_{1.05}Mn_{1.96}O_4$ cathodes were assembled in experimental batteries, and these were either charged to 4.10 V, 4.15 V, and 4.21 V, or first charged to 4.40 V and then discharged to 4.10 V, 4.00 V, and 3.95 V. The selected voltages correspond to the starts or ends of the charge–discharge plateaux, as shown in Fig. 3. Here 1 mol L^{-1} $LiPF_6$-EC/DMC (1:1, v/v) was used as the electrolyte to minimize the effect of residual solvent in the $Li_{1.05}Mn_{1.96}O_4$ cathode, because DMC (dimethyl carbonate) is more volatile than DEC and may interfere less with the signals from the SEI. Fig. 4 shows the FTIR spectrum of 1 mol L^{-1} $LiPF_6$-EC/DMC (1:1, v/v), which is very similar to that of 1 mol L^{-1} $LiPF_6$-EC/DEC (1:1, v/v) shown in Fig. 1.

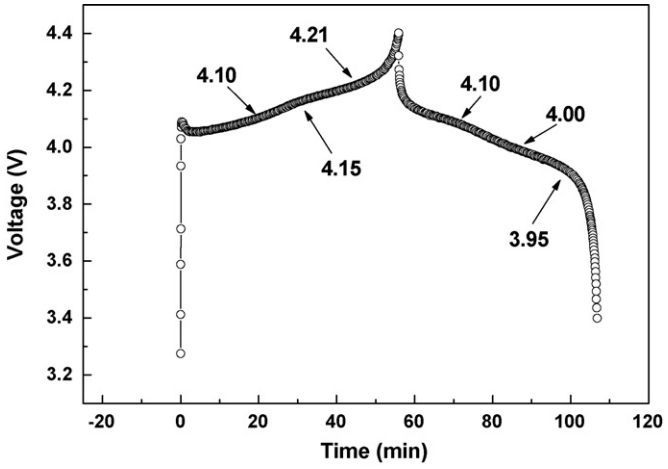

Fig. 3. The initial galvanostatic charge–discharge curves of $Li_{1.05}Mn_{1.96}O_4$ at a current density of 0.4 mA cm^{-2}. The electrolyte is 1 mol L^{-1} $LiPF_6$-EC/DMC (1:1, v/v).

The absorptions of the $Li_{1.05}Mn_{1.96}O_4$ cathodes in different charge states are shown in Fig. 5. The absorption bands located at

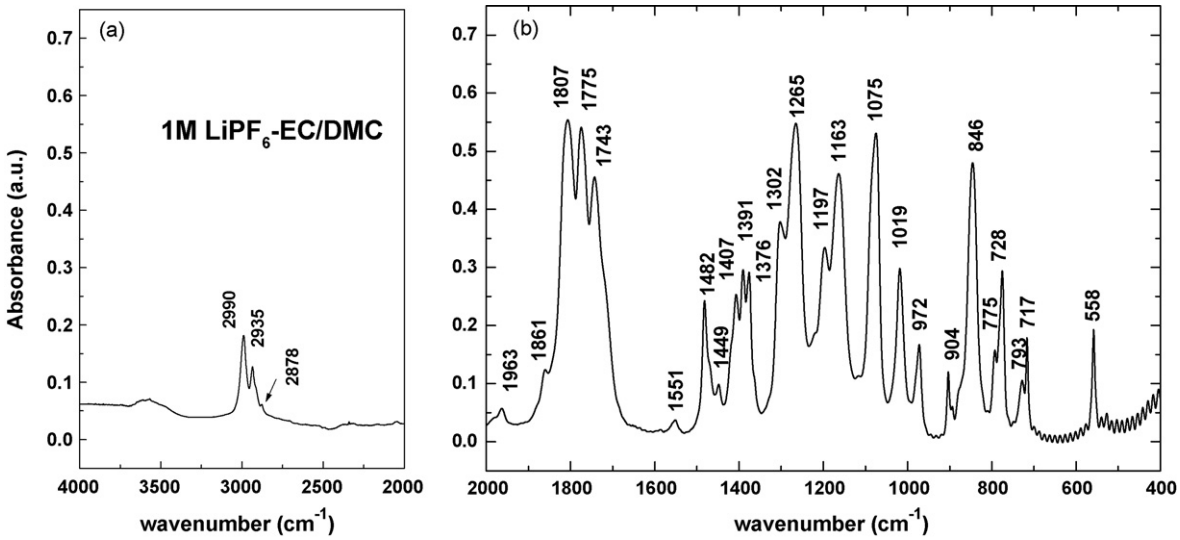

Fig. 4. FTIR spectrum of non-aqueous organic electrolyte 1 mol L^{-1} $LiPF_6$-EC/DMC in different regions: (a) 4000–2000 cm^{-1}; (b) 2000–400 cm^{-1}.

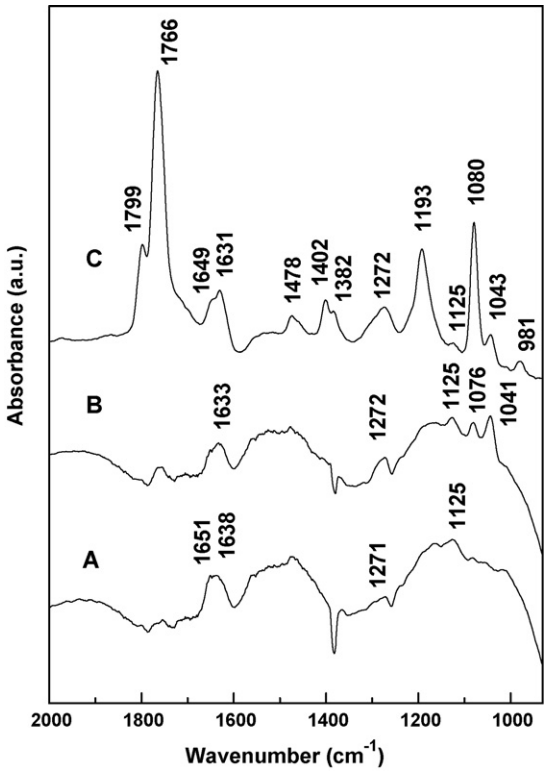

Fig. 5. FTIR spectra of $Li_{1.05}Mn_{1.96}O_4$ cathodes charged to different states in 1 mol L^{-1} $LiPF_6$-EC/DMC (1:1, v/v): (A) 4.10 V; (B) 4.15 V; (C) 4.21 V.

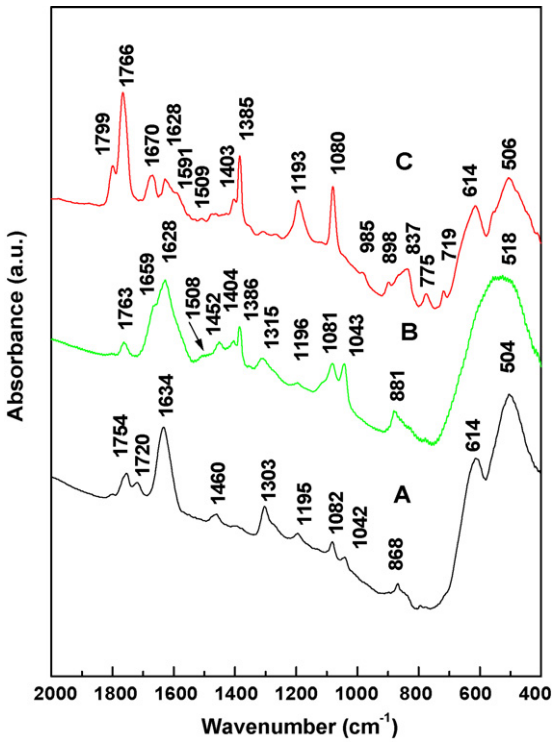

Fig. 6. FTIR spectra of $Li_{1.05}Mn_{1.96}O_4$ cathodes charged to 4.40 V and then discharged to different states: (A) 4.10 V; (B) 4.00 V; (C) 3.95 V. The electrolyte is 1 mol L^{-1} $LiPF_6$-EC/DMC (1:1, v/v).

550–450 cm^{-1} and 650–600 cm^{-1} are the characteristic vibrations of $LiMn_2O_4$ [37], indicating that the spinel structure is retained during the charging process. The FTIR spectra of $Li_{1.05}Mn_{1.96}O_4$ charged from 4.10 V to 4.21 V were found to be clearly different from that of the electrolyte in Fig. 4. At 4.10 V and 4.15 V, the CO_2 asymmetric bending of R-CO_3Li is identified at 722 cm^{-1} and 672 cm^{-1}, while at 4.21 V the CO_3 bending of R-CO_3Li is identified at 879 cm^{-1}. For all three charge states, new absorption bands located at 1631–1651 cm^{-1} are assigned to the CO_2 stretching of R-CO_3Li, while those located at 1271 (1272) cm^{-1} and 1125 cm^{-1} are assigned to the CO stretching of R-CO_3Li. When the charge voltage exceeds 4.15 V, an additional C–O–C stretching mode [38] is detected at 1041 (1043) cm^{-1}. On further charging to 4.21 V, new $CH(CH_3)$ asymmetric bending and CO stretching modes of R-CO_3Li are detected at 1382 cm^{-1} and 981 cm^{-1}, respectively. This implies that some electrolyte may be gradually decomposed during the charge process, and the formation of the SEI on the $Li_{1.05}Mn_{1.96}O_4$ becomes ever more distinct with increasing charge voltage. Therefore, the FTIR vibration of R-CO_3Li intensifies on going from 4.10 V to 4.21 V. Assignments of all of the absorption bands of $Li_{1.05}Mn_{1.96}O_4$ during the charge process are listed in Table 2.

According to Aurbach et al. [8,32], R-CO_3Li mainly originates from reactions between the solvents and the lithium metal foil, as described by Eqs. (8) and (9). They believe that the R-CO_3Li may first be formed on the lithium anode, and then migrates with the electrolyte, and ultimately adheres to the cathode. In fact, R-CO_3Li may also come from the reaction of Li^+ with the solvents, as described by Eq. (10):

$$2EC + 2e^- + 2Li^0 \rightarrow (CH_2OCO_2Li)_2 \downarrow + CH_2CH_2 \uparrow \quad (8)$$

$$DMC + 2e^- + 2Li^0 \rightarrow 2CH_3OCO_2Li \downarrow + CH_3CH_3 \uparrow \quad (9)$$

$$DMC + 2e^- + 2Li^+ \rightarrow LiCH_2CO_3CH_2Li \downarrow \quad (10)$$

In this study, it has been proved that the direct formation of R-CO_3Li on $Li_{1.05}Mn_{1.96}O_4$ is possible. On the other hand, it would be very difficult for even a small quantity of R-CO_3Li formed on the lithium anode to migrate through the membrane to the $Li_{1.05}Mn_{1.96}O_4$ cathode in just the initial cycle.

Table 2
Comparison of FTIR peaks of surface layers on $Li_{1.05}Mn_{1.96}O_4$ at different charge states in 1 M $LiPF_6$-EC/DMC.

Charge states	Peak positions (cm^{-1})			
	EC/DMC	$LiPF_6$	$LiMn_2O_4$	R-CO_3Li
1 M $LiPF_6$-EC/DMC	2990–2878m, 1963w, 1807s, 1775s, 1743s, 1551w, 1482m, 1449w, 1407m, 1391m, 1376m, 1302s, 1265s, 1197m, 1163s, 1075s, 972m, 904m, 793m, 775m, 728w, 717m	1019m, 846s, 558m		
4.10 V	1754w		650–600m 550–450s	1651m, 1638m, 1272m, 1125w, 722m, 672m
4.15 V	1756w, 1076m		650–600m 550–450s	1633m, 1272m, 1125w, 1041m, 722m, 672m
4.21 V	1799s, 1766vs, 1478m, 1402m, 1193s, 1080s, 776w, 716m	850m, 557s	650–600m 550–450s	1649m, 1631m, 1382m, 1271m, 1125w, 1043m, 981w, 897m

Note: w: weak, m: middle, s: strong, vs: very strong.

Table 3
Comparison of FTIR peaks of surface layers on $Li_{1.05}Mn_{1.96}O_4$ at different discharge states in 1 M $LiPF_6$-EC/DMC.

Discharge states	Peak positions (cm^{-1})			
	EC/DMC	Li_2CO_3	$LiMn_2O_4$	R-CO_3Li
4.10 V	1754w, 1720w, 1303m, 1195w, 1082w	868w	614s, 504s	1634s, 1460w, 1042w
4.00 V	1763w, 1404w, 1386m, 1196w, 1081m	1508vw, 1452w	518s	1659sh, 1628s, 1315m, 1043m, 881m
3.95 V	1799m, 1766s, 1080s, 1193s, 1385s, 1403sh, 775m, 719w,	898–837m, 1509vw	614s, 506s	1670m, 1628m, 1591sh, 985w, 898–837m

Note: w: weak; vw: very weak; m: middle; s: strong; sh: shoulder.

3.4. Formation and evolution of the SEI in the initial discharge process

The absorptions of $Li_{1.05}Mn_{1.96}O_4$ cathodes in different discharge states are shown in Fig. 6. At 4.10 V, a weak but distinct peak appears at 868 cm^{-1}. When the cathode is discharged to 4.00 V, weak peaks at 1508 cm^{-1} and 1452 cm^{-1} are detected. On further discharging to 3.95 V, absorption bands at 1509 cm^{-1} and 837–898 cm^{-1} can be easily identified, which may be assigned to the CO_3 bending of Li_2CO_3. All of these characteristic peaks indicate the formation of Li_2CO_3 during the initial discharge process. As previously reported by Aurbach et al. [32,39], if there is a trace of H_2O in the electrolyte, R-CO_3Li will decompose to form Li_2CO_3 and CO_2, as described by Eq. (11). The by-product CO_2 will then react with Li^+ to form more Li_2CO_3 according to Eq. (12). Since the discharge cathodes were carefully washed with DME, no absorption peaks due to $LiPF_6$ are observed in the FTIR spectra. However, the vibration modes of residual solvent can still be detected, as listed in Table 3:

$$2\text{R-CO}_3\text{Li} + \text{H}_2\text{O} \rightarrow \text{Li}_2\text{CO}_3\downarrow + 2\text{ROH} + \text{CO}_2\uparrow \quad (11)$$

$$2\text{CO}_2 + 2\text{Li}^+ + 2\text{e}^- \rightarrow \text{Li}_2\text{CO}_3\downarrow + \text{CO}\uparrow \quad (12)$$

Assignments of all of the absorption bands of $Li_{1.05}Mn_{1.96}O_4$ during the discharge process are listed in Table 3. Taking these together with the assignments listed in Table 2, it is evident that during the initial charge process an SEI with R-CO_3Li as the major component is formed on the $Li_{1.05}Mn_{1.96}O_4$ cathode, while during the initial discharge process the formation of Li_2CO_3 gradually becomes evident, and the co-existence of R-CO_3Li and Li_2CO_3 is detected.

4. Conclusions

With the aid of Fourier-transform infrared spectroscopy, the formation and evolution of the SEI on $Li_{1.05}Mn_{1.96}O_4$ cathode have been studied. It has been found that during the charge–discharge process, the SEI can be directly formed on the $Li_{1.05}Mn_{1.96}O_4$ cathode. It is mainly composed of R-CO_3Li and Li_2CO_3, and is very similar to those formed on carbon anodes. In the initial cycle, the formation of R-CO_3Li begins at 4.10 V during the charge process, and becomes more distinct with increasing charge voltage. The formation of Li_2CO_3 begins at 4.10 V during the discharge process, and becomes more distinct with decreasing discharge voltage. The SEI becomes more evident in subsequent cycles.

Acknowledgments

The authors thank the National 973 Program (grant no. 2009CB220100), the Beijing Excellent Talent Support Program (grant no. 20071D1600300396), and the Teaching & Research Fund of BIT (grant no. 20060542012) for financial support.

References

[1] A.N. Dey, B.P. Sullivan, J. Electrochem. Soc. 117 (1970) 222.
[2] R. Fong, U.V. Sacken, J.R. Dahn, J. Electrochem. Soc. 137 (1990) 2009.
[3] E. Peled, H. Straze, J. Electrochem. Soc. 124 (1977) 1030.
[4] E. Peled, J. Electrochem. Soc. 126 (1979) 2047.
[5] Y. Matsumura, S. Wang, J. Mondori, J. Electrochem. Soc. 142 (1995) 2914.
[6] E. Goren, O. Chusid, D. Aurbach, J. Electrochem. Soc. 138 (1991) L6.
[7] D. Aurbach, M.L. Daroux, P.W. Faguy, E. Yeager, J. Electrochem. Soc. 135 (1988) 1863.
[8] D. Aurbach, M.L. Daroux, P.W. Faguy, E. Yeager, J. Electrochem. Soc. 134 (1987) 1611.
[9] D. Aurbach, Y. Ein-Eli, B. Markovsky, A. Zaban, S. Luski, Y. Carmeli, H. Yamin, J. Electrochem. Soc. 142 (1995) 2882.
[10] S.-I. Pyun, Y.-G. Ryu, J. Electroanal. Chem. 455 (1998) 11.
[11] M. Lu, H. Cheng, Y. Yang, Electrochim. Acta 53 (2008) 3539.
[12] S.-H. Kang, D.P. Abraham, A. Xiao, B.L. Lucht, J. Power Sources 175 (2008) 526.
[13] S. Leroy, H. Martinez, R. Dedryvere, D. Lemordant, D. Gonbeau, Appl. Surf. Sci. 253 (2007) 4895.
[14] S.S. Zhang, J. Power Sources 163 (2007) 713.
[15] L.W. Zhao, I. Watanabe, T. Doi, S. Okada, J.-i. Yamaki, J. Power Sources 161 (2006) 1275.
[16] H. Nakahara, S. Nutt, J. Power Sources 160 (2006) 1355.
[17] H. Buqa, A. Wursig, J. Vetter, M.E. Spahr, F. Krumeich, P. Novak, J. Power Sources 153 (2006) 385.
[18] J.-C. Panitz, U. Wietelmann, M. Wachtler, S. Strobele, M. Wohlfahrt-Mehrens, J. Power Sources 153 (2006) 396.
[19] V. Eshkenazi, E. Peled, L. Burstein, D. Golodnitsky, Solid State Ionics 170 (2004) 83.
[20] F. Galobardes, C. Wang, M. Madou, Diam. Relat. Mater. 15 (2006) 1930.
[21] K.-C. Moller, H.J. Santner, W. Kern, S. Yamaguchi, J.O. Besenhard, M. Winter, J. Power Sources 119–121 (2003) 561.
[22] S.-B. Lee, S.-I. Pyun, Carbon 40 (2002) 2333.
[23] P. Novak, F. Joho, R. Imhof, J.-C. Panitz, O. Haas, J. Power Sources 81/82 (1999) 212.
[24] D. Aurbach, A. Zaban, A. Schechter, Y. Ein-Eli, E. Zinigrad, B. Markovsky, J. Electrochem. Soc. 142 (1995) 2873.
[25] A. Lisowska-Oleksiak, Solid State Ionics 119 (1999) 205.
[26] J.Z. Li, H. Li, Z.X. Wang, L.Q. Chen, X.J. Huang, J. Power Sources 107 (2002) 1.
[27] G.C. Chuang, J. Power Sources 104 (2002) 7.
[28] R. Dedryvere, H. Martinez, S. Leroy, D. Lemordant, F. Bonhomme, P. Biensan, D. Gonbeau, J. Power Sources 174 (2007) 462.
[29] H. Ota, T. Akai, H. Namita, S. Yamaguchi, M. Nomur, J. Power Sources 119–121 (2003) 567.
[30] K. Araki, N. Sato, J. Power Sources 124 (2003) 124.
[31] S. Yoon, J.-J. Cho, Electrochem. Commun. 9 (2007) 801.
[32] D. Aurbach, J. Power Sources 89 (2000) 206.
[33] K. Edstrom, T. Gustafsson, J.O. Thomas, Electrochim. Acta 50 (2004) 397.
[34] Y. Bai, C. Wu, F. Wu, G.Q. Wang, Trans. Nonferrous Met. Soc. China 16 (2006) 402.
[35] C. Wu, F. Wu, L.Q. Chen, X.J. Huang, Solid State Ionics 152/153 (2001) 335.
[36] JCPDS No. 35-0782 (1984).
[37] C. Wu, Z. Wang, F. Wu, L. Chen, X. Huang, Solid State Ionics 144 (2001) 277.
[38] D. Aurbach, Y. Ein-Ely, A. Zaban, J. Electrochem. Soc. 141 (1994) L1.
[39] D. Aurbach, Y. Ein-Eli, O. Chusid, Y. Cameli, Y. Babai, H. Yamain, J. Electrochem. Soc. 141 (1994) 603.